On stellar limb darkening and exoplanetary transits.

Ian D. Howarth*

Dept. Physics & Astronomy, UCL, Gower Street, London WC1E 6BT, UK

ABSTRACT

This paper examines how to compare stellar limb-darkening coefficients evaluated from model atmospheres with those estimated from photometry. Limb-darkening coefficients derived from light-curve analyses using approximate limb-darkening 'laws' are shown to be dependent on system geometry, while different characterizations of a given model atmosphere can give quite different numerical results. These issues are examined in the context of exoplanetary transits, which offer significant advantages over traditional binary-star eclipsing systems in the investigation of stellar limb darkening. 'Like for like' comparisons between light-curve analyses and new model-atmosphere results, mediated by synthetic photometry, are conducted for a small sample of stars. Agreement between the resulting synthetic-photometry/atmosphere-model (SPAM) limb-darkening coefficients and empirical values ranges from very good to quite poor, even though there is only a small dispersion in fundamental stellar parameters.

1 INTRODUCTION

Stellar limb darkening is the wavelength-dependent decrease in specific intensity, $I_\lambda(\mu)$, with decreasing μ, where $\mu = \cos\theta$ and θ is the angle between the surface normal and the line of sight;[1][2] in the context of model atmospheres, it is, in principle, significantly more sensitive to input physics than are integral quantities, such as the emergent flux.

Until rather recently, the only important opportunity to compare models and observations of limb darkening for the distant stars has been through eclipsing-binary systems, but there the comparison has been hindered both by the rather weak dependence on limb darkening of the light-curves, and by degeneracies with other model parameters. As a consequence, normal practice among light-curve analysts has been to *assume* some description of limb darkening, based on stellar-atmosphere results; any errors in the description are liable to be concealed by small adjustments to fitted free parameters.

New observational techniques have begun to allow the direct investigation of limb darkening (and hence more sensitive tests of model-atmosphere calculations) under other circumstances. Optical interferometry has opened the way to direct imaging of stellar surfaces beyond the solar system for a handful of stars with the largest angular diameters (e.g., Aufdenberg, Ludwig & Kervella 2005), and microlensing light-curves are also capable of probing the intensity distribution of the lensed source (e.g., Witt 1995; Zub et al. 2011), albeit usually only crudely (Dominik 2004). However,

the focus of the present paper is on the role of limb darkening in exoplanetary transits, which are likely to yield many more results in the coming years than any other technique.

In many respects, star+exoplanet systems are close to being idealised eclipsing binaries: it is often reasonable to assume that the photometric properties of the parent star are unaffected by the transiting planet (i.e., no tidal distortion, 'reflection' effect, or gravity darkening), and that the secondary (planet) is completely dark, and spherical. These assumptions reduce the number of geometric unknowns to be determined from the light-curve to only two (the ratio of the two radii, and the minimum impact parameter);[3] this allows a more critical examination of limb darkening than in star+star systems. With an anticipated torrent of data of extremely high quality from satellites such as *Kepler*, it is therefore timely to revisit the comparison of limb-darkening coefficients (LDCs) from model-atmosphere and light-curve analyses, as has already been recognized by several authors (e.g. Southworth 2008; Pál 2008; Claret 2009).

The plan of this paper is as follows: Section 2 reviews limb-darkening 'laws' and fitting techniques (including a new flux-conserving least-squares methodology), stressing the spread in numerical coefficients that can arise even when characterizing a given model-atmosphere intensity distribution with a given law. Section 3 examines the LDCs extracted from light-curve analyses, emphasizing the range in numerical coefficients that can arise from characterizing a given surface-brightness distribution under different geometries. With the background that (i) the numerical values of coefficients determined from model atmospheres depend on the fitting method, and (ii) coefficients determined

---

[1] Under some circumstances, limb *brightening* can occur.
[2] The specific intensity, referred to as the radiance in other contexts, is the rate of energy flow per unit area, per unit time, per unit wavelength interval, per unit solid angle. Expressing I_λ as a function of a single angle μ makes the implicit assumption of azimuthal symmetry of the radiation field.

[3] Of course, the remaining orbital properties have (normally second-order) affects on the light-curve, but are usually better determined from radial-velocity obervations than from photometry.

from light-curves vary with impact parameter, Section 4 outlines a 'like for like' comparison of model-atmosphere limb-darkening results with high-quality exotransit photometry, and presents illustrative results.

2   CHARACTERIZING LIMB DARKENING

In photometric analyses, it is still impractical to invert observed light-curves in order to recover detailed stellar surface-brightness distributions. Rather, in this context limb darkening is habitually represented by some *ad hoc* 'law' with one or, at most, two free parameters, which may be optimized as part of the fitting process.[4] In order to facilitate comparison of light-curve results with model-atmosphere calculations, model intensities are often represented with the same parametrizations.

2.1   Functional forms

Historically, the first limb-darkening law to be developed was the analytical solution for an atmosphere in which the source function is linear in optical depth:

$$I_\lambda(\mu) = I_\lambda(1) \left[1 - u(1 - \mu)\right] \qquad (1)$$

(Schwarzschild 1906), where the wavelength dependence of u is implicit (although $u = 0.6$ at all wavelengths for a grey atmosphere; Milne 1921). This linear law is the universally adopted one-parameter representation of limb darkening.

More-realistic atmosphere models do not have analytical functional representations of actual limb darkening. Following the work of Kopal (1949), a quadratic law of the form

$$I(\mu) = I(1) \left[1 - u_1(1 - \mu) - u_2(1 - \mu)^2\right] \qquad (2)$$

has been widely adopted as a characterization of model-atmosphere calculations and. It is of particular importance in modelling exotransit photometry using Monte-Carlo Markov-Chain (MCMC) techniques, since it allows for analytical calculation of light-curves with good computational efficiency (Mandel & Agol 2002).

While eqtns. 1 and 2 are convenient in the analysis of light-curves,[5] a significantly more accurate representation of model-atmosphere results is achieved with the four-coefficient fit introduced by Claret (2000):

$$I(\mu) = I(1) \left[1 - \sum_{n=1}^{4} a_n \left(1 - \mu^{n/2}\right)\right]. \qquad (3)$$

This form reproduces intensities from model atmospheres to ~1 part in 1000 over a wide range of parameter space (e.g., Howarth 2011), although it isn't practical to estimate numerical values of the coefficients from photometry.

---

[4] In practice, even 'two-parameter' fits still allow only one coefficient to be determined reliably; see the discussion in Section 4.
[5] A number of other limb-darkening laws have been proposed; cf., e.g., Díaz-Cordovés & Giménez (1992)

2.2   Fitting model-atmosphere intensities.

Although linear and quadratic limb-darkening laws may not give particularly accurate functional descriptions of model-atmosphere intensities, it is nonetheless necessary to represent them in this way in order to compare with observationally derived LDCs. However, even for a given limb-darkening law, the characterization of model-atmosphere results using different fitting techniques can result in quite different values for the coefficients

2.2.1   *LS1: least squares with $I(1)$ constrained*

Rewriting eqtn. 1 as

$$I_\lambda(\mu)/I_\lambda(1) = \left[1 - u(1 - \mu)\right],$$

gives a one-parameter formulation straightforwardly solved by least squares for u, using input model-atmosphere values of $I(\mu)$. The intercept of the linear fit is implicitly constrained such that $\hat{I}(1)$, the value of $I(1)$ evaluated from the fitted law, is fixed at model-atmosphere value. The quadratic equivalent is

$$I_\lambda(\mu)/I_\lambda(1) = \left[1 - u_1(1 - \mu) - u_2(1 - \mu)^2\right],$$

2.2.2   *LS2: least squares with $I(1)$ free*

Relaxing the constraint that $\hat{I}(1) \equiv I(1)$ gives laws that can be again be solved in a trivial least-squares exercise, with $\hat{I}(1)$ as an additional free parameter:

$$I_\lambda(\mu) = \hat{I}_\lambda(1) \left[1 - u(1 - \mu)\right]$$

(linear; in practice, both sides may be divided by $I(1)$),

$$I_\lambda(\mu) = \hat{I}_\lambda(1) \left[1 - u_1(1 - \mu) - u_2(1 - \mu)^2\right]$$

(quadratic).

2.2.3   *Flux-conserving fit: FC1*

The physical flux F_λ is related to the specific intensity through

$$F_\lambda = 2\pi \int_0^1 I_\lambda(\mu)\mu \, d\mu \qquad (4)$$
$$= 4\pi H_\lambda$$

where H_λ is the Eddington flux (the first-order moment of the radiation field). The integration of eqtn. 4 using an analytical limb-darkening law to represent $I_\lambda(\mu)$, with coefficients determined by least squares, will not normally recover the physical flux exactly. To address this, we can impose the condition that

$$F_\lambda = 2\pi \int_0^1 \hat{I}_\lambda(\mu)\mu \, d\mu;$$

that is,

$$F_\lambda = \pi\hat{I}(1)\left[1 - u/3\right]$$
$$F_\lambda = \frac{2\pi\hat{I}(1)}{12}\left[6 - 2u_1 - u_2\right]$$
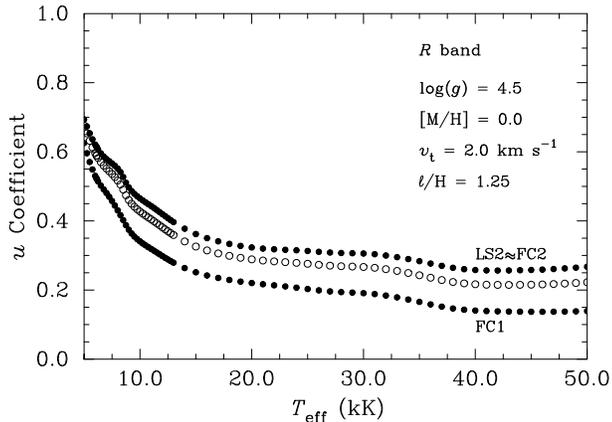
Figure 1. Comparison of linear limb-darkening coefficients determined from model atmospheres by different numerical techniques (cf. Section 2), as a function of effective temperature. Open circles are LS1 results.

Figure 2. Limb darkening in the H and U bands, for a 4kK model. The thick 'lines' are individual model-atmosphere intensities, shown as points which merge together at this scale. The fitted 4-coefficient limb-darkening laws are shown drawn through the points. Straight lines show the linear limb-darkening laws for the H band, with coefficients determined by flux conservation (labelled FC1) and by flux-conserving least squares (cf. Section 2.2).

in the linear and quadratic cases, respectively. Then requiring $\hat{I}(\mu)$ to equal $I(\mu)$ at some arbitrary $\mu = x$ we find, for the linear law,

$$u = \frac{\pi I_\lambda(x) - F_\lambda}{(\pi I_\lambda(x)/3) + (x - 1)F_\lambda}. \qquad (5)$$

Wade & Rucinski (1985) chose $x = 1$, whence

$$u = 3\left[1 - F_\lambda/\left(\pi I_\lambda(1)\right)\right]$$

(noting the Wade & Rucinski's "angle-averaged" [astrophysical] flux is F/π in the nomenclature adopted here). In effect, the choice of x fixes the intercept of the linear law, with the constraint of flux conservation then fixing the slope. The equivalent algebra for the quadratic law follows from selecting any two values $\mu = x_1, x_2$ at which $\hat{I}(\mu)$ is equal to $I(\mu)$, giving a pair of simultaneous equations that can readily be solved for u_1, u_2. Wade & Rucinski (1985), and subsequent authors, used $x_1 = 1, x_2 = 0.1$ (values which are also adopted here), but again these are more or less arbitrary choices.

2.2.4 *Flux-conserving least squares: FC2*

The weakness of the standard flux-conserving approach is the lack of a compelling physical argument to select any particular x value for the normalization (other than requiring the intensities to be everywhere positive; e.g., requiring $0 \geqslant u \geqslant 1$).

Rather than making an arbitrary choice of x, we can instead introduce the more objective requirement of minimising the sum of the squares of the differences between model and fitted intensities while still requiring flux to be conserved. For a linear law it is convenient first to determine u by minimising $\sum \left(\hat{I}(\mu) - I(\mu)\right)^2$, where

$$\hat{I}_\lambda(\mu) = \frac{3F_\lambda}{\pi}\left[\frac{1 - u(1 - \mu)}{3 - u}\right]$$

and to then evaluate
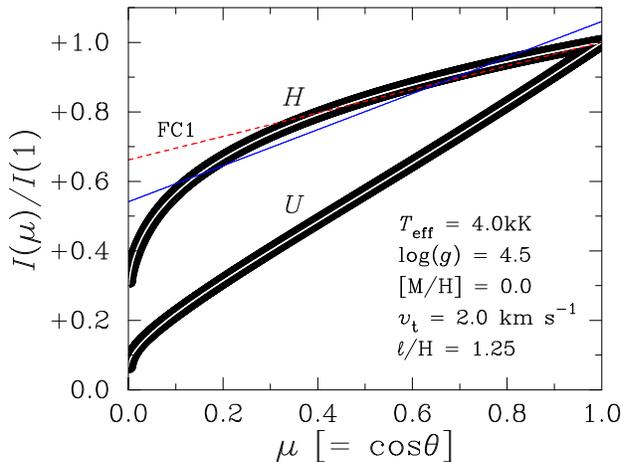
$$\hat{I}_\lambda(1) = \frac{3F_\lambda}{\pi(3 - u)}.$$

Corresponding results for the quadratic law are

$$\hat{I}_\lambda(\mu) = \frac{6F_\lambda}{\pi}\left[\frac{1 - u_1(1 - \mu) - u_2(1 - \mu)^2}{6 - 2u_1 - u_2}\right]$$

$$\hat{I}_\lambda(1) = \frac{6F_\lambda}{\pi(6 - 2u_1 - u_2)}.$$

Not surprisingly, this newly introduced approach of flux-conserving least squares generally yields numerical coefficients close to those found using the LS2 method.

2.3 Other numerical factors

The foregoing numerical methods can (and do) yield substantially different LDC values, even for the standard linear and quadratic representations of a given, fixed, intensity distribution, as is illustrated by Figs. 1 and 2. For a given intensity distribution, in the optical wavelength regime the FC1 u coefficient is usually the smallest numerically; LS2 and FC2 u coefficients are very similar, and relatively large; and the LS1 coefficient is intermediate.

When characterizing model-atmosphere results, the density and distribution of angles at which intensities are calculated, and the weighting scheme, will also influence the numerical values of limb-darkening coefficients (e.g., Díaz-Cordovés & Giménez 1992; Claret 2008). Of course, the physics used in constructing the model atmosphere is critical, too. The limb-darkening coefficients used throughout this paper were computed using the ATLAS9 line-blanketed LTE model-atmosphere code (Kurucz 1993), as ported to GNU-linux systems by Sbordone, Bonifacio & Castelli (2007), with the Opacity Distribution Functions described by Howarth (2011). Solar abundances ([M/H] = 0.0), a microturbulent velocity of $v_\mathrm{t} = 2$ km s^{-1}, and mixing-length parameter $\ell/H = 1.25$ were adopted unless noted otherwise.

Intensities were computed for $\mu = 0.001$ to 1 at steps of 0.001,[6] and equally weighted when fitting functional forms.

The dispersion in coefficient values introduced simply by numerical techniques poses the question: which procedure is most appropriate for comparing model-atmosphere results with observational determinations of limb darkening? To answer this question it is necessary first to examine just what it is that is measured from transit observations.

3   INFERENCES FROM EXOTRANSIT PHOTOMETRY

Photometric observations of exoplanetary transits record, essentially, the variation of $I_\lambda(p)/F_\lambda$ along a chord, where $p = \sqrt{1 - \mu^2}$ is the impact parameter. The extent to which this variation is representative of the global limb darkening must depend on the minimum impact parameter, $p_{\min}$; on how faithfully the chosen parametrization of the limb darkening matches the intensities on those parts of the star that are occulted; and how well it extrapolates to those parts that are not.

Given that simple linear and quadratic limb-darkening laws give only approximate representations of actual intensity distributions, it might be anticipated that LD coefficients determined from light-curves must, at some level, suffer systematic biasses depending on $p_{\min}$, and that those coefficients must therefore fail to correspond directly to any equivalent, single-valued, characterization of model-atmosphere results.

To demonstrate and quantify these effects, model transit light-curves have been generated for a range of stellar temperatures and passbands. Limb darkening was represented in the light-curve calculations by eqtn. 3, with coefficients determined by least squares (i.e., for practical purposes, the model-atmosphere results were represented almost exactly). The geometry was set by choosing a ratio of planetary to stellar radii of 1:10, representative of 'hot Jupiter' systems commonly observed to transit (although the output limb-darkening results are insensitive to this ratio), with the minimum impact parameter varied over the range 0–0.95. The resulting light-curves were then solved for basic geometrical parameters, and for linear or quadratic LDCs. These calculations were performed using a modified version of JKTEBOP (Southworth 2004a,b), which is itself based on Etzel's EBOP code (Etzel 1981; Popper & Etzel 1981).

3.1   Linear law

Figure 3 shows a selection of the results, and demonstrates that, in this parameter space, linear LDCs derived from photometry systematically increase with increasing impact parameter, by up to ∼0.2 (∼60%). This behaviour is straightforward to understand: in the optical regime $\partial I/\partial \mu$ decreases with increasing μ, so that any transit that is not central (i.e., inclination $i \neq 90°$) samples a relatively steep part of the limb-darkening law. A linear approximation to

that law must therefore yield a linear limb-darkening coefficient that is, in general, larger than that derived from a central transit.

Figure 2 illustrates this point by showing model-atmosphere results, and linear approximations, for a 4kK model. The intensity in the U band is very nearly a linear function of μ, so any characterization will yield similar numerical values for the u coefficient. This is confirmed both in that least-squares and flux-conserving approaches yield similar results in this passband, and in that the u coefficient derived photometrically is insensitive to impact parameter (upper-left panel of Fig. 3). This contrasts with H-band results; the intensity there is a strongly non-linear function of angle, and any diagnostic that characterizes only small μ values must yield a larger u coefficient than that characterizing the entire centre-to-limb variation. Fig. 3 shows this to be the case.

Fig. 3 also shows the linear limb-darkening coefficients obtained by fitting the input intensity distributions using flux-conserving (FC1) and flux-conserving least-squares (FC2) techniques, which bracket the range of numerical values derived directly from the model atmospheres. In this parameter space, these coefficients also almost bracket the corresponding photometric LDCs which suggests a simple, if rough-and-ready, means of comparing observational and model-atmosphere parametrizations. Furthermore, if one had to choose a *single,* linear limb-darkening coefficient to compare with photometric results, then the FC1 value is probably the least poor option; for randomly inclined orbits, smaller impact parameters are more probable than larger ones (and observational selection effects also favour higher orbital inclinations), and photometrically determined limb darkening coefficients are generally closest to the FC1 LDC in this case.[7]

3.2   Quadratic law

The variations in linear limb-darkening coefficient are present *a fortiori* for the quadratic coefficients, although here the interpretation is less straightforward because of the well-known strong correlation between u_1 and u_2, evident in the left-hand panel of Fig. 4 (see also Fig. 2 in Southworth 2008). Pál (2008) and Kipping & Bakos (2011a) point out that this correlation is largely removed through a rotation onto new principal axes,

$$w_1 = u_1 \cos\phi - u_2 \sin\phi,$$
$$w_2 = u_2 \cos\phi + u_1 \sin\phi, \qquad (6)$$

with $\phi \simeq 40°$. Results rotated to these co-ordinates are shown in the right-hand panel of Fig. 4, and confirm that, while the w_1 values show a large (impact-parameter-dependent), w_2 is more nearly constant.

The correspondence between the photometric and model-atmosphere results is less straightforward than with the linear law; the single-valued representations of limb darkening show no simple relationship to the photometrically-determined equivalents (notwithstanding rough quantitative similarities). Nevertheless, the small dispersion

---

[6] The intensities were calculated in detail, not 'densified' from a sparser grid.

[7] This conclusion is supported by results from many more synthetic light-curves than are reported on here.
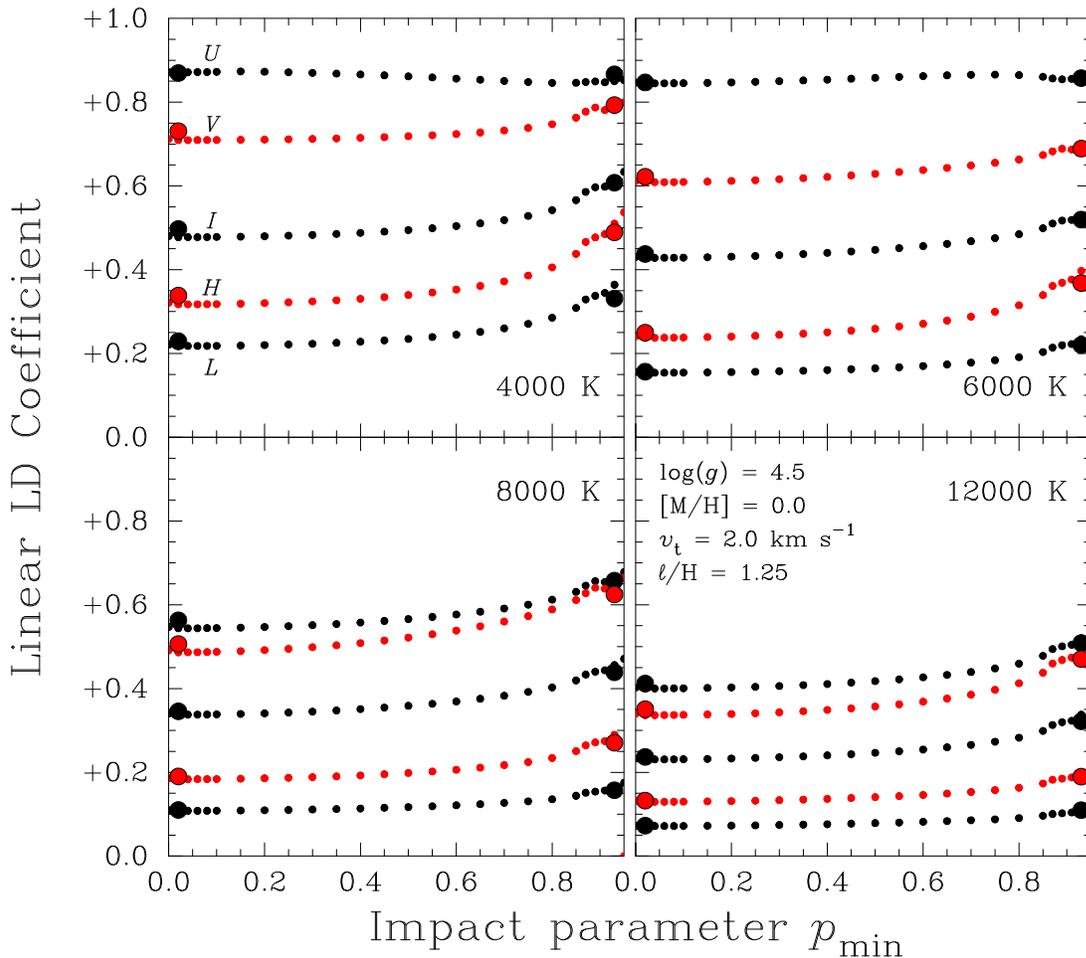
Figure 3. Photometrically determined linear limb-darkening coefficients (small dots), for fixed input limb darkening, in the Johnson-Cousins-Glass *UVIHL* passbands (cf. Section 3.1). Larger dots show corresponding linear limb-darkening coefficients determined directly from the *same* input model-atmosphere intensity distributions using flux-conserving and flux-conserving least-squares fitting (FC1, FC2: left, right, respectively), plotted at arbitrary impact parameters.

found for the w_2 coefficient in *both* observational and model-atmosphere characterizations of limb darkening indicates that this should be the parameter of choice when making comparisons.

4 COMPARING MODEL-ATMOSPHERE AND PHOTOMETRIC LIMB-DARKENING

The foregoing sections emphasize that different characterizations of model-atmosphere results can give quite different numerical results (e.g., Fig. 1); and that light-curve analyses, using, of necessity, approximate limb-darkening 'laws', yield LDCs that vary with transit geometry (e.g., Fig. 3). In order to examine the relationship between empirical, photometric LDCs and theoretical model-atmosphere values, it is therefore necessary to devise a method ensuring a fair comparison.

The most direct way to perform such a 'like for like' comparison is to adapt the methods used in Section 3, i.e., to generate model light-curves for well-studied systems, using as inputs the empirically determined geometric parameters, coupled to model-atmosphere intensity distribu-

tions (in practice, approximated by eqtn. 3) for the 'known' stellar parameters. This synthetic photometry can then be solved for the geometric parameters and LDCs, using the same simplified limb-darkening law adopted in the observational photometric analysis. The resulting hybrid synthetic-photometry/atmosphere-model (SPAM) LDCs can reasonably be compared directly with empirical values.[8]

This approach has been used to investigate two illustrative datasets: the eight stars with *Kepler* data analysed by Kipping & Bakos (2011a,b), and the multiwavelength study of HD 209458 by Knutson et al. (2007; see also Southworth 2008, Claret 2009). Synthetic light-curves were generated with 1000 data points through transit (phases ±0.05; errors are not quoted on any results because the analysis is essentially deterministic).

---

[8] Using a simplified description of limb darkening in the fitting step drives the inferred geometric parameters away from their input values, but by usually unimportant amounts (e.g., radii change by less than 1%).
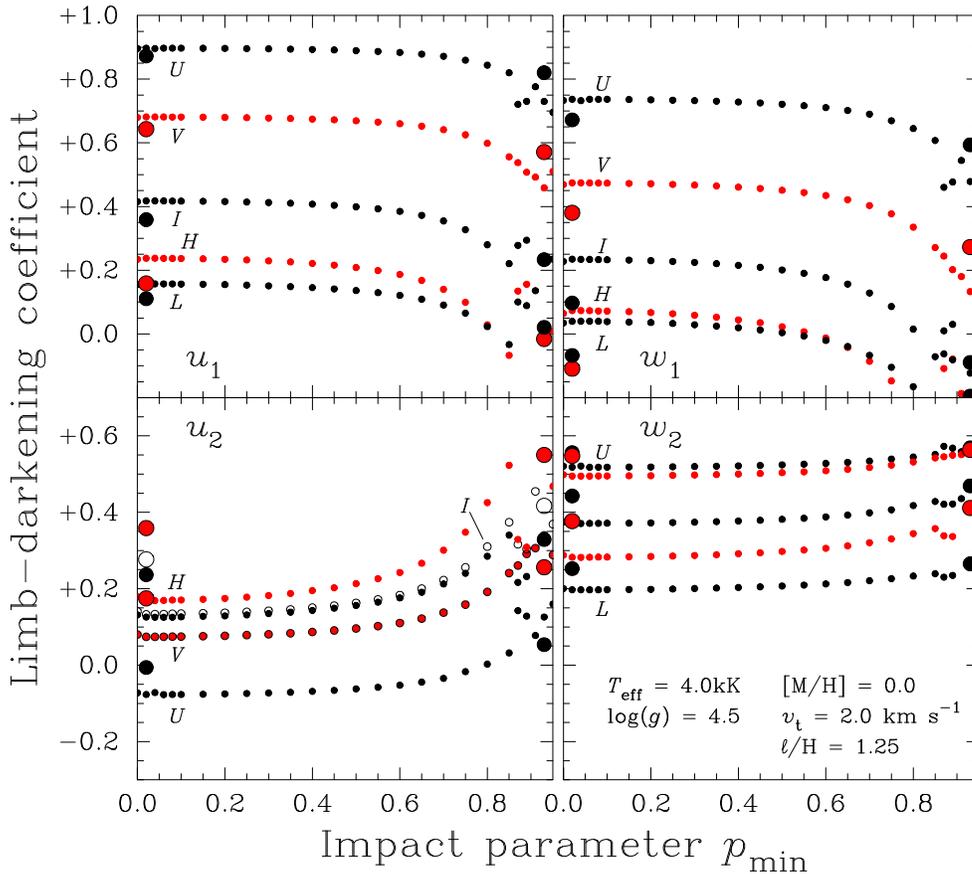
Figure 4. Photometrically determined quadratic limb-darkening coefficients for a 4kK model in the Johnson-Cousins-Glass *UVIHL* passbands. Left-hand panels, u_1, u_2 coefficients (eqtn. 2); right-hand panels, rotated w_1, w_2 coefficients (Section 3.2). Larger dots show corresponding quadratic limb-darkening coefficients determined directly from the *same* input model-atmosphere intensity distributions using flux-conserving and flux-conserving least-squares fitting (left, right, respectively; FC1, FC2; Section 2.2), plotted at arbitrary impact parameters.

4.1 Kepler targets

Kipping & Bakos (2011a,b) derived quadratic limb-darkening coefficients for the eight *Kepler* targets they studied. Their Monte-Carlo Markov-Chain results are reproduced here in Fig. 5.

Custom model atmospheres were computed for each system as described in Section 2.3; adopted stellar parameters are summarized in Table A1. This group of stars samples a fairly small range in atmospheric properties (T_{eff} = 5647 : 6297 K, $\log g$ = 3.96 : 4.59, [M/H] = −0.55 : +0.33), which is reflected in a rather small range in model-atmosphere and SPAM LDCs. It's therefore somewhat surprising that agreement between empirical LDCs and those from the SPAM approach (or from direct fitting to model atmospheres[9]) varies from excellent (Kepler-6) to statistically unacceptable (e.g., Kepler-5).

There is a suggestion that the extent of agreement correlates with temperature; the SPAM LDCs for the three coolest stars fall within the cloud of the best-fitting 90% of solutions, while those for the three hottest lie (just) out-side.[10] The trend is for the cloud of empirical values to move towards smaller (u_1, u_2) values with increasing temperature, compared to the model-atmosphere results. It's unclear why the empirical results should show so much greater variation than the models, suggesting that this apparent trend may simply be an artefact of the small sample, or that some additional factor plays an unexpectedly important role.

4.2 HD 209458

Baseline parameters of T_{eff} = 6113 K (Casagrande 2010), $\log g$ = 4.50, [M/H] = +0.03 (Sousa et al. 2008), v_t = 2 km s^{-1}, ℓ/H = 1.25 were adopted to construct the reference model atmosphere and intensities for HD 209458. Broad-band limb-darkening was calculated by assuming 'top hat' response functions for the photometric passbands of the Knutson et al. HST observations. The principal results are summarized in Table A2

Additional models were run for T_{eff} = 5913, 6313; $\log g$ = 4.2, 4.8; ℓ/H = 0.5; v_t = 0, 4 km s^{-1}; and [M/H] =

---

[9] In general, the SPAM results are closest to the FC1 direct characterization of intensities.

[10] The cooler stars in this sample are also those with higher gravities and metallicities, so temperature is not necessarily the key parameter.
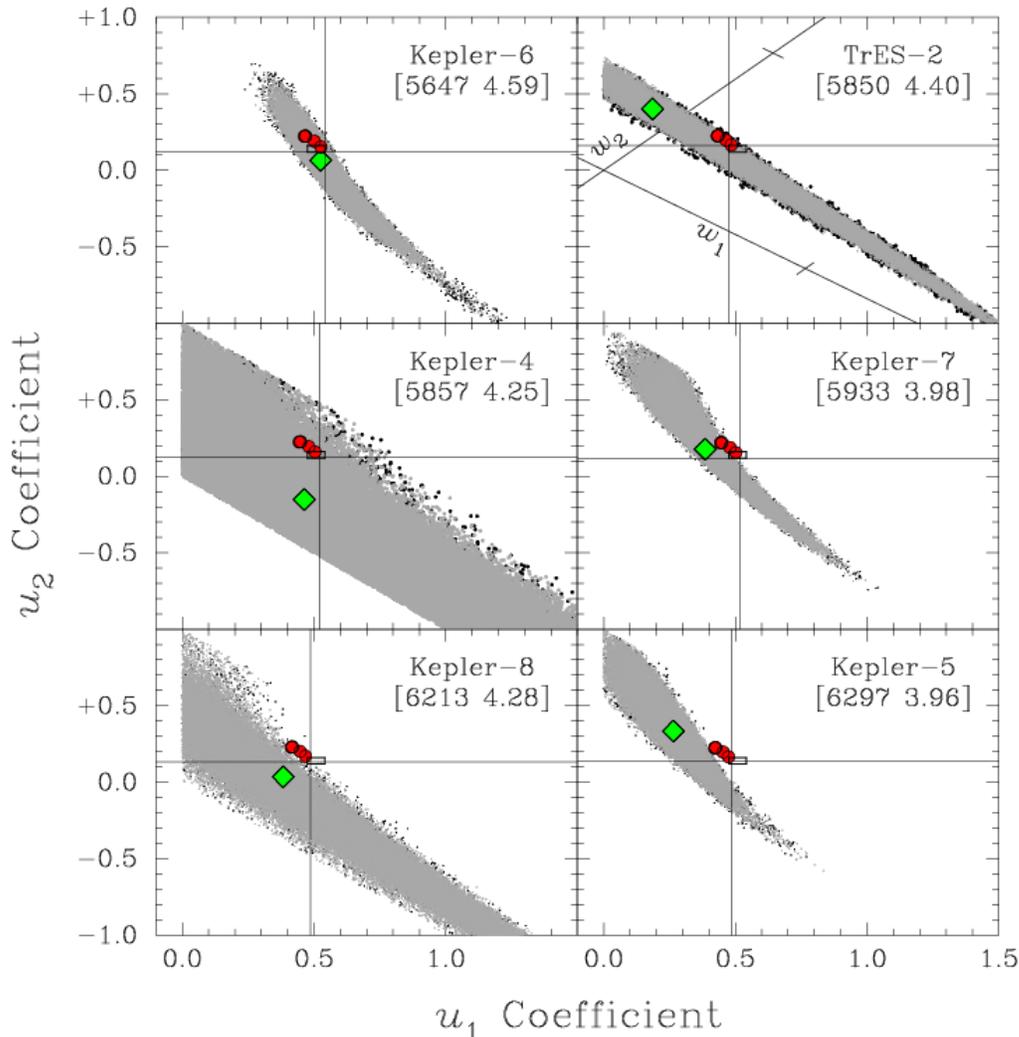
Figure 5. Quadratic limb-darkening coefficients determined by Kipping & Bakos (2011a,b) from *Kepler* photometry compared with model-atmosphere results. Panels are identified by star name, $T_{\rm eff}$, and $\log g$. Bands of grey points show the projection onto the (u_1, u_2) plane of the 90% of MCMC results yielding the smallest χ^2 values, which overlay the best 95% results (black points, not visible in all frames because this figure is a projection of multiparameter modelling onto a specific 2D plane). Green diamonds show the minimum-χ^2 solutions. Red dots show fits to model-atmosphere intensities (left to right: FC2/LS2 [indistinguishable at this scale], LS1, FC1), while horizontal and vertical lines indicate the SPAM solutions. The small rectangle shown in each panel (and most easily seen by zooming in on the on-line version) encompasses *all* the SPAM solutions, and is included to provide an indication of the rather small scale of uncertainties resulting from any uncertainties in input stellar parameters. The rotated w_1, w_2 axes (eqtn. 6) are shown in the Tres-2 panel, for reference; by design, most of the variance in the MCMC results is in w_1.

$-0.4, +0.4$. These ranges allow for quite generous uncertainties in parameters for this well-studied system. The extremes in linear LDCs from the models are for the low-$T_{\rm eff}$ and high-gravity models (numerically largest and smallest coefficients, respectively), and these models are used to illustrate plausible 'error bars' on the SPAM coefficients in Figs. 6 and 7.

Fig. 6 shows results for linear coefficients. The discrepancies between model-atmosphere and photometric results already noted by Claret (2009; see also Southworth 2008), on the basis of older models,[11] persist in the new analysis.

The comparison for quadratic coefficients is shown in Fig. 7. The variation with wavelength of both u_1 and u_2 coefficients is much less for the SPAM coefficients than is found empirically. However, both sequences run almost parallel to the rotated w_1 axis, and agreement in the better-determined w_2 parameter is tolerable at all wavelengths. [12]

[11] The principal cause of the minor quantitative differences between the results shown in Fig. 6 appears to be the different treatments of convection adopted here and by Kurucz (1993; the source of Claret's models).

[12] The observational uncertainties can't be straightforwardly propagated from $\sigma(u_{1,2})$ to $\sigma(w_{1,2})$ because of the strong correlation between u_1 and u_2. It should also be noted that the error bars in Fig. 7 represent the 68% dispersion in parameter values obtained from MC replications (Southworth, personal communication); they therefore can't be compared directly to the dispersion in results shown in Fig. 5, which show parameters from the 90/95% of solutions with the smallest overall χ^2 values.
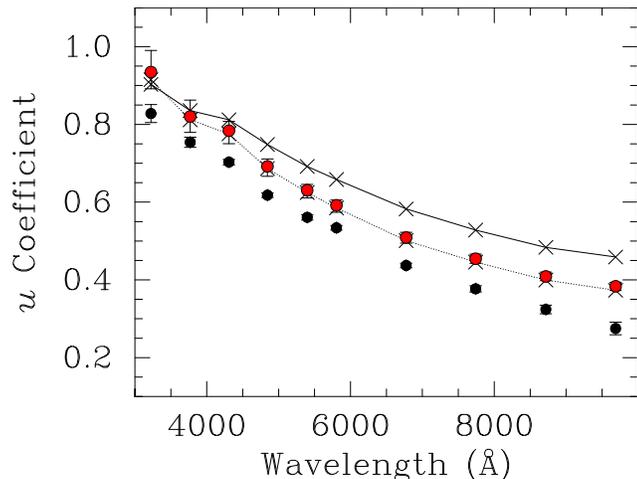
Figure 6. Comparison of linear limb-darkening coefficients determined observationally for HD 209458 (lower set of black points, from Southworth 2008) and SPAM calculations (upper set of red points). The 'error bars' on the model-atmosphere results are the result of varying input stellar parameters (see Section 4.2 for details). Continuous and dotted lines connect LS2 and FC1 model-atmosphere results, respectively.
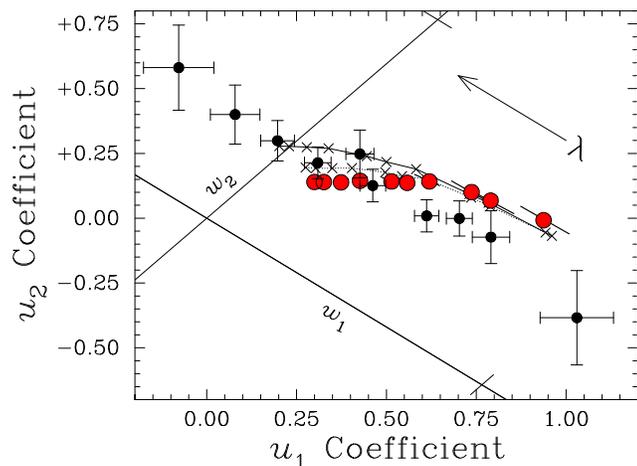

Figure 7. Comparison of quadratic limb-darkening coefficients for HD 209458. Black points with error bars, empirical values from Southworth (2008); red points, SPAM results (Section 4.2). Continuous and dotted lines connect LS2 and FC1 model-atmosphere results, respectively.

In particular, for the ~675 nm passband, which is close to the effective wavelength of the Kepler results, the agreement is reasonably good, $[(w_1, w_2) = (0.234, 0.385), (0.099, 0.363)$ for SPAM and light-curve coefficients, respectively]. This is in contrast to the Kepler results for stars at similar effective temperatures (but is consistent with the result that it is the higher-gravity stars that show the best agreement between models and observations).

5   SUMMARY AND CONCLUSIONS

Different methods of fitting a given limb-darkening law to a given model-atmosphere intensity distribution lead to quite different numerical coefficients. Furthermore, the limb-

darkening coefficients determined from photometry of exoplanetary transits are functions of minimum impact parameter, and can't reliably be compared directly to any of the standard model-atmosphere characterizations.

A more direct comparison can be made if the model intensities are translated into observer space, through the medium of synthetic light-curves. The resulting synthetic-photometry/atmosphere-model (SPAM) limb-darkening coefficients are not single-valued, but *can* be compared directly with empirical results. [If one had to choose a traditional single-valued representation of model-atmosphere results, then at optical wavelengths closest agreement with the SPAM results is generally obtained with the standard (FC1) flux-conserving method, which also yields the smallest value of the linear limb-darkening coefficient.]

For the commonly used quadratic limb-darkening law, most of the variation in different model-atmosphere fits is along the w_1 axis, with much smaller dispersions in the w_2 direction. Since w_1 is also defined as the axis that maximizes dispersion in observational (Monte-Carlo) results, the most sensitive comparison between models and observations is in the value of w_2.

New model-atmosphere calculations, analysed with the SPAM approach, show mixed results. Agreement with empirical Kepler LDCs is good in some cases (differences in w_2 less than 0.06 in four out of six systems), but not in others. There is a hint of a possible temperature dependence in the extent of disagreement for these targets, with cooler stars showing better agreement. However, at similar effective wavelengths HST results for HD 209458 (which is at the hotter end of the range of Kepler targets) agree well with models; there are discrepancies at longer and short wavelengths, though again with fair agreement in w_2. Since gravity (and metallicity) correlate with temperature for the Kepler sample, and since HD 209458 is both high-temperature and high-gravity in the context of that sample, this might be taken as an indication that agreement is better at higher gravities (with temperature as a secondary factor). However, the ranges in all quantities characterizing the atmospheres are so small as to render such conclusions speculative at this stage. Forthcoming results from Kepler, and other missions, should enlarge the parameter space, and permit better discrimination of where models and observations do and do not agree.

REFERENCES

Aufdenberg, J.P., Ludwig, H.-G., Kervella, P., 2005, ApJ, 633 , 424
Casagrande, L., Ramírez, I., Meléndez, J., Bessell, M., Asplund, M., A&A, 512, 54
Claret, A., 2000, A&A, 363, 1081
Claret, A., 2008, A&A, 482, 259
Claret, A., 2009, A&A, 506, 1335

Díaz-Cordovés, J., Giménez, A., 1992, A&A, 259, 227

Dominik, M., 2004, MNRAS, 352, 1315

Etzel, P. B., 1981, in Carling, E. B., Kopal, Z., eds, NATO ASI Ser. C, 69, Photometric and Spectroscopic Binary Systems. Dordrecht, p. 111

Howarth, I.D., 2011 MNRAS, 413, 1515

Kipping, D., Bakos, G., 2011a, ApJ, 730, 50

Kipping, D., Bakos, G., 2011a, ApJ, 733, 36

Knutson, H.A., Charbonneau, D., Noyes, R.W., Brown, T.M., Gilliland, R.L., 2007, ApJ, 655, 564

Kopal, Z., 1949, HCO Circ. 454

Kurucz, R.L., 1993, CD-ROM 12, Smithsonian Astrophysical Observatory

Mandel, K., Agol, E., 2002, ApJ, 580, L171

Milne E.A., MNRAS 81, 361

Pál, A., 2008, MNRAS, 390, 281P

Popper, D.M., Etzel, P.B., 1981, ApJ, 86, 102

Sbordone, L., Bonifacio, P., Castelli, F., 2007, in Convection in Astrophysics (IAU Symp. 239), p. 71

Schwarzschild K., 1906, Nachrichten von der Gesellschaft der Wissenschaften zu Göttingen, Mathematisch-Physikalische Klasse, p. 43

Sousa, S.G., Santos, N.C., Mayor, M., Udry, S., Casagrande, L., Israelian, G., Pepe, F., Queloz, D., Monteiro, M.J.P.F.G., 2008, A&A, 487, 373

Southworth, J., 2004a, MNRAS, 351, 1277

Southworth, J., 2004b, MNRAS, 355, 986

Southworth, J., 2008, MNRAS, 386, 1644

Wade, R.A., Rucinski, S.M., 1985, A&AS, 60, 471

Witt, H.J., ApJ, 449, 42

Zub, M., Cassan, A., Heyrovský, D., Fouqué, P., Stempels, H.C., et al., 2011, A&A, 525, 15

APPENDIX A: FIT RESULTS

This paper has been typeset from a TeX/ LaTeX file prepared by the author.

Table A1. Limb-darkening results: Kepler photometry. For each star, the physical parameters used in the model-atmosphere calculations are first listed, followed by the resulting 4-parameter Kepler-band limb-darkening coefficients (eqtn. 3). Subsequent columns list the SPAM coefficients, determined by fitting synthetic light-curves generated from the 'known' system parameters; the best-fit empirical photometric coefficients; and, for reference, coefficients determined directly from the model-atmosphere intensity distributions. All necessary stellar & system parameters are adopted from Kipping & Bakos (2011a,b).

| | Photometry (Synthetic) | Photometry (Observed) | Model-atmosphere fits | | | |
			LS1	LS2	FC1	FC2
Kepler-4	$T_{\rm eff} = 5857$ K, $\log g = 4.25$, $[{\rm M/H}] = +0.17$, $v_{\rm t} = 2$ km s^{-1}, $\ell/H = 1.25$.					
$a_n, n = 1, 4$	+7.63788E-01	−7.97285E-01	+1.40090E+00	−5.86378E-01		
linear, u	+0.6080		+0.6252	+0.6491	+0.5828	+0.6491
quad, u_1	+0.5201	$+0.61^{+0.59}_{-0.39}$	+0.4805	+0.4480	+0.5035	+0.4481
quad, u_2	+0.1230	$-0.21^{+0.52}_{-0.68}$	+0.1931	+0.2256	+0.1586	+0.2256
Kepler-5	$T_{\rm eff} = 6297$ K, $\log g = 3.96$, $[{\rm M/H}] = +0.03$, $v_{\rm t} = 2$ km s^{-1}, $\ell/H = 1.25$.					
$a_n, n = 1, 4$	+7.34699E-01	−7.94487E-01	+1.43212E+00	−6.20527E-01		
linear, u	+0.5564		+0.6011	+0.6265	+0.5566	+0.6267
quad, u_1	+0.4877	$+0.25^{+0.13}_{-0.12}$	+0.4537	+0.4248	+0.4739	+0.4250
quad, u_2	+0.1377	$+0.37^{+0.25}_{-0.27}$	+0.1966	+0.2254	+0.1654	+0.2253
Kepler-6	$T_{\rm eff} = 5647$ K, $\log g = 4.59$, $[{\rm M/H}] = +0.33$, $v_{\rm t} = 2$ km s^{-1}, $\ell/H = 1.25$.					
$a_n, n = 1, 4$	+8.20192E-01	−9.18046E-01	+1.53037E+00	−6.26480E-01		
linear, u	+0.5967		+0.6436	+0.6664	+0.6025	+0.6665
quad, u_1	+0.5415	$+0.55^{+0.13}_{-0.11}$	+0.5011	+0.4675	+0.5262	+0.4675
quad, u_2	+0.1189	$+0.01^{+0.26}_{-0.27}$	+0.1901	+0.2240	+0.1527	+0.2240
Kepler-7	$T_{\rm eff} = 5933$ K, $\log g = 3.98$, $[{\rm M/H}] = +0.11$, $v_{\rm t} = 2$ km s^{-1}, $\ell/H = 1.25$.					
$a_n, n = 1, 4$	+7.48602E-01	−7.78844E-01	+1.38072E+00	−5.77728E-01		
linear, u	+0.5850		+0.6205	+0.6439	+0.5790	+0.6440
quad, u_1	+0.5191	$+0.34^{+0.16}_{-0.13}$	+0.4795	+0.4480	+0.5017	+0.4481
quad, u_2	+0.1183	$+0.33^{+0.26}_{-0.34}$	+0.1881	+0.2196	+0.1546	+0.2195
Kepler-8	$T_{\rm eff} = 6213$ K, $\log g = 4.28$, $[{\rm M/H}] = -0.55$, $v_{\rm t} = 2$ km s^{-1}, $\ell/H = 1.25$.					
$a_n, n = 1, 4$	+7.13647E-01	−7.27611E-01	+1.35455E+00	−5.92941E-01		
linear, u	+0.5817		+0.5980	+0.6240	+0.5525	+0.6241
quad, u_1	+0.4864	$+0.41^{+0.55}_{-0.25}$	+0.4474	+0.4176	+0.4675	+0.4179
quad, u_2	+0.1337	$+0.11^{+0.44}_{-0.83}$	+0.2008	+0.2305	+0.1701	+0.2304
Tres-2	$T_{\rm eff} = 5850$ K, $\log g = 4.40$, $[{\rm M/H}] = +0.15$, $v_{\rm t} = 2$ km s^{-1}, $\ell/H = 1.25$.					
$a_n, n = 1, 4$	+6.97192E-01	−6.67832E-01	+1.29178E+00	−5.62467E-01		
linear, u	+0.6238		+0.6117	+0.6366	+0.5676	+0.6368
quad, u_1	+0.4754	$+0.52^{+0.44}_{-0.34}$	+0.4644	+0.4344	+0.4846	+0.4346
quad, u_2	+0.1608	$+0.06^{+0.37}_{-0.48}$	+0.1964	+0.2264	+0.1659	+0.2264

Table A2. Limb-darkening results: HD 209458. System parameters and observed LDCs are from Southworth (2008). Stellar parameters $T_{\rm eff}$ = 6113 K (Casagrande 2010), $\log g$ = 4.50, [M/H] = +0.03 (Sousa et al. 2008), $v_{\rm t}$ = 2 km s^{-1}, ℓ/H = 1.25. Columns follow the model of Table A1, with rows grouped by HST wavelength in nm.

| | | Photometry (Synthetic) | Photometry (Observed) | Model-atmosphere fits | | | |
				LS1	LS2	FC1	FC2
HST-320;	$a_n, n = 1, 4$	+4.58205E-01	-7.02251E-01	+1.97519E+00	-7.98143E-01		
linear, u		+0.9346	+0.828±0.023	+0.9064	+0.9029	+0.9151	+0.9029
quad, u_1		+0.9373	+1.030±0.102	+0.9438	+0.9607	+0.9428	+0.9607
quad, u_2		−0.0076	−0.384±0.182	−0.0500	−0.0681	−0.0553	−0.0681
HST-375;	$a_n, n = 1, 4$	+6.43615E-01	-9.36895E-01	+2.09622E+00	-8.88657E-01		
linear, u		+0.8204	+0.754±0.013	+0.8283	+0.8356	+0.8118	+0.8356
quad, u_1		+0.7901	+0.791±0.052	+0.7809	+0.7844	+0.7888	+0.7844
quad, u_2		+0.0680	−0.073±0.012	+0.0632	+0.0596	+0.0460	+0.0596
HST-430;	$a_n, n = 1, 4$	+6.15746E-01	-8.44919E-01	+2.00870E+00	-8.87838E-01		
linear, u		+0.7839	+0.703±0.007	+0.8005	+0.8118	+0.7758	+0.8118
quad, u_1		+0.7370	+0.703±0.036	+0.7283	+0.7312	+0.7360	+0.7312
quad, u_2		+0.1006	−0.001±0.068	+0.0964	+0.0933	+0.0797	+0.0933
HST-485;	$a_n, n = 1, 4$	+6.33987E-01	-6.21291E-01	+1.55033E+00	-7.10907E-01		
linear, u		+0.6919	+0.618±0.006	+0.7276	+0.7482	+0.6865	+0.7483
quad, u_1		+0.6197	+0.612±0.034	+0.5962	+0.5826	+0.6109	+0.5826
quad, u_2		+0.1418	+0.009±0.062	+0.1754	+0.1894	+0.1511	+0.1894
HST-540;	$a_n, n = 1, 4$	+7.10040E-01	-7.19161E-01	+1.47157E+00	-6.49635E-01		
linear, u		+0.6307	+0.561±0.007	+0.6684	+0.6919	+0.6248	+0.6919
quad, u_1		+0.5578	+0.426±0.039	+0.5240	+0.4999	+0.5437	+0.5000
quad, u_2		+0.1364	+0.248±0.092	+0.1927	+0.2171	+0.1622	+0.2171
HST-580;	$a_n, n = 1, 4$	+7.20922E-01	-6.88211E-01	+1.34528E+00	-5.92544E-01		
linear, u		+0.5917	+0.534±0.006	+0.6322	+0.6583	+0.5852	+0.6584
quad, u_1		+0.5141	+0.462±0.036	+0.4756	+0.4453	+0.4967	+0.4455
quad, u_2		+0.1417	+0.126±0.063	+0.2089	+0.2394	+0.1770	+0.2393
HST-678;	$a_n, n = 1, 4$	+7.67414E-01	-7.43741E-01	+1.22290E+00	-5.25063E-01		
linear, u		+0.5090	+0.437±0.006	+0.5520	+0.5824	+0.5011	+0.5826
quad, u_1		+0.4267	+0.309±0.037	+0.3799	+0.3392	+0.4044	+0.3395
quad, u_2		+0.1442	+0.214±0.061	+0.2295	+0.2696	+0.1935	+0.2695
HST-775;	$a_n, n = 1, 4$	+7.82449E-01	-7.91226E-01	+1.16704E+00	-4.88230E-01		
linear, u		+0.4545	+0.377±0.008	+0.4964	+0.5282	+0.4458	+0.5286
quad, u_1		+0.3737	+0.197±0.047	+0.3240	+0.2785	+0.3494	+0.2790
quad, u_2		+0.1384	+0.299±0.078	+0.2299	+0.2741	+0.1929	+0.2739
HST-873;	$a_n, n = 1, 4$	+7.95398E-01	-8.55463E-01	+1.17721E+00	-4.90744E-01		
linear, u		+0.4088	+0.324±0.011	+0.4498	+0.4837	+0.3996	+0.4838
quad, u_1		+0.3259	+0.079±0.069	+0.2751	+0.2289	+0.3030	+0.2290
quad, u_2		+0.1396	+0.400±0.114	+0.2331	+0.2774	+0.1930	+0.2773
HST-971;	$a_n, n = 1, 4$	+7.63034E-01	-7.89085E-01	+1.07318E+00	-4.49903E-01		
linear, u		+0.3835	+0.275±0.016	+0.4242	+0.4588	+0.3732	+0.4591
quad, u_1		+0.2997	−0.078±0.098	+0.2496	+0.2021	+0.2753	+0.2025
quad, u_2		+0.1398	+0.581±0.164	+0.2330	+0.2782	+0.1958	+0.2780